METALLOGENIC POTENTIAL EVALUATION OF PAN-AFRICAN GRANITES FROM BAFOUSSAM (WEST-CAMEROON): INSIGHTS FROM GEOCHEMICAL APPROACH

Abstract

Bafoussam granites, is located in western Cameroon, on the N50E branch of the Central Cameroon Shear Zone. The main aim of this study is to identify its metallogenic potential based on petrographic and geochemical data. Petrographic data include K-feldspar megacryst granites, two–mica granites, biotite granites, amphibolites and mylonites. The evaluation of the mineralization potential reveals that these granitoids plot in oxidized fields, overlapping the specialized and non-specialized fields; thus indicating that they are not entirely barren. They tend to fall between the specialized and non–specialized granitoid fields, showing that they are not all fertiles. From a metallogenic point of view, histograms and box–plots of geochemical data of the Bafoussam granitoids, enrichment Mn, Ta, Mg, Ca, Mo, Ti, Fe, Na, Sc, V, Ni, Rb, Sn, Ba et Yb whose average abundance are higher than those of the crust. This pluton exhibits significant potential for Ba, Sn, Mo, Rb and REE mineralization.

Introduction:-

Various exploration approach including structural controls, geological and geochemical mapping amongs others have been used to assess granitic bodies' mineralization potential [1, 2, 3]. Granites concentrate important volumes of metals, such as Mo, Rb, Sn, Li, Zr, Th, Be, Li, Nb, Ta, Cs, W, Cu, and Au [1, 2] which spatially and temporally distributed within their different types. For example, I–type granites concentrate Ag, Au, Cu, Fe, Ga, Mo and Zn while S–type granites concentrate Sn, U and W [1, 2, 3]. Numerous granitic bodies cropout along the N50E branch of the Central Cameroun Shear Zone (CCSZ). Their origin and evolution as well as their emplacement ages and regimes have been largely debated by [4, 5, 6, 7, 8, 9, 10]. However their mineralization potentials remain poorly understood. Some recent research works revealed that many of these rocks are potentially rich in major (e.g., Zn, Fe, U, Cu, Pb, Ag, Sn, W), minor (e.g., Re, Bi, Te, Cd, and Sc, Sb), and rare (e.g., Ta, Nb, Li, Be, Zr, and Lanthanides) metals [1, 2, 11].

This paper presents a cas in which petrographic data, histograms and box plot representations from geochemical data are used to evaluate and highlight the mineralization potential of the Bafoussam granites.

Key words:-
xxxxxxxxxx

Keywords:- Bafoussam granites, Metallogenic Potential, Central Cameroon Shear Zone, West Cameroon.

II. Geological setting

Pan–African granitoids are widely distributed throughout the Central African Fold Belt (CAFB) in Cameroon, specialy in its southeastern part. Their relative emplacement ages range from the early stage of orogenic deformation (640 Ma, [4]), after which they were metomorphosed into orthogneisses, to the late uplift stage of global geotectonic evolution (572 Ma, [4]). They can be subdivided into three main types related to the orogenic deformation phases: (i) pre– to syn–D_1 granitoids (640-613Ma), (ii) syn– to post–D_2 granitoids (613–572 Ma), and (iii) post–orogenic granitoids (>542 Ma,) [4, 12, 13]. In western Cameroon, some of the Pan–African plutons including the Bafoussam, Dschang and Batié granitoids have been subject of detailed petrologic studies [4, 14, 15, 16, 17] which described the aforementioned granitoids as syn– to post–collisional, emplaced during the D_2 and D_3 Pan–African deformation phases. The study of the metallogenic aspect of these Pan–African granitods is becoming one of the main scientific research target [1, 2, 18, 19]. Such studies by [18] in Banyo, [19] in Mayo Darley and [1, 2] in Dschang and Batié, highlighted oxides, hydroxides, trace element and rare earth elements enrichment in Pan–African granitoids. These results thus emphasize the necessity of intensifying research works for potentially major, minor and rare metals enrichment in Pan–African granitoids. This thus reinforce the relevance of further studies on the Bafoussam granitoids, given their geological similarities and their belonging to this potentially mineralized CAFB [20] for the base metal enrichment potential.

III. Methods

Fourteen fresh samples collected from the main lithologies (Fig. 1b) were used for thin sections and their detailed petrographic analyses were carry out under a crossed polarizes light microscope in the Laboratory of Geosciences, Natural Resources and Environment of the Univerity of Douala. Fourteen whole–rock geochemical data from [14] were used for the samples barrenness or fertility assessment in discrimination diagrams with respect to specific elements/metals, according to established metallogenic granitoids protocols [21]. The geochemical data were statistically processed using the GeoChemical Data Toolkit (GCDkit 6.0) software of [22], supported by R 3.6.0 (for Windows), to identify positive and/or negative anomalies in the data that have implications for mineralization. Results for selected metals/elements from the geochemical data were tested for normal distribution using histograms and box plots in which the median value (50th percentile) is denoted by a bold line within the box, Q_1 (25th percentile) and Q_3 (75th percentile) respectively representing the lower and upper quartiles. The interquartile Range (IQR), corresponds to the difference between Q_3 and Q_1, serving as a measure to detect outliers within a specified window of 1.5 x IQR. For the determination of elements with positive concentrations, the statistical threshold formula was Threshold = Q_3 +1.5 x IQR, while for negative anomalies the statistical threshold formula was Threshold = Q_1 – 1.5 x IQR. These fomulars were applied following the [23] approach, therefore establishing an upper threshold for anomaly detection. Data that exceeded or fell below this threshold were classified as anomalous, with values above the threshold signifying positive anomalies and those below indicating negative anomalies.

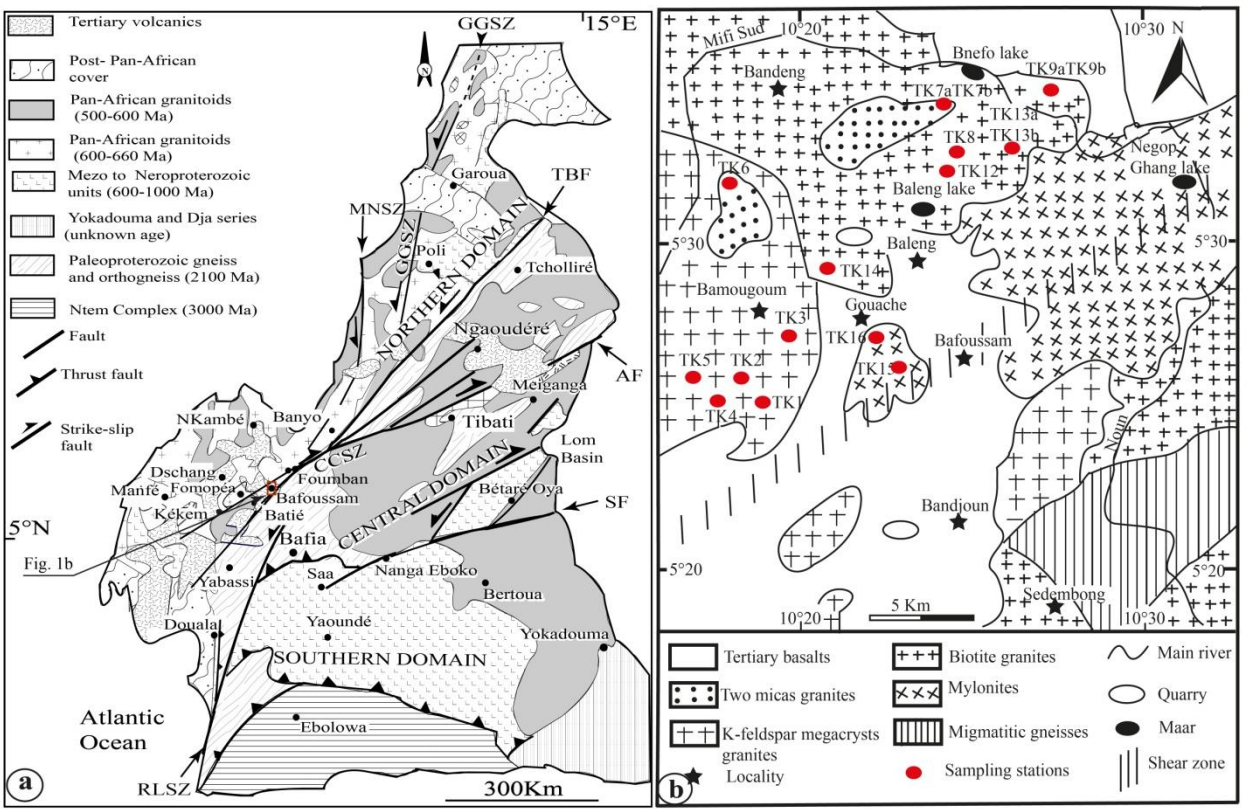

AF, Adamawa Fault; CCSZ, Central Cameroon Shear Zone; TBF, Teholiré Banyo Fault: SF, Sanaga Fault; RLSZ, Rocher du Loup Shear Zone; GGSZ, Godé Gormaya Shear Zone; MNSZ, Mayo Nolti Shear Zone

Figure 1. (a) Pan–African lithostructural map of Cameroon and location of the study. (b)Sketch of the study area adapted from [16] showing the sampling stations

IV. Results

IV.1. Petrography

Five petrographic types including K–feldspar megacrysts granites, two–mica granites, biotite granites, amphibolites, and mylonites (protomylonites and mylonites) were recorded (Fig. 2).

K-feldspar megacrysts granites

At Bamougoum, granitoids with K–feldspar megacrysts outcrop as blocks on hilltops and hillslopes and, in places, as slabs in valley and riverbeds (Fig. 2a). Some K–feldspar megacrysts may attain 4 cm major axis and 2 cm minor axis. Thin sections (Fig. 2b) exhibit a granular, porphyritic texture made up of plagioclase (40%), quartz (20%), potassium feldspar (15%), biotite (9%), and opaque minerals (2%).

Two–mica granites

Two–mica granites cropout as slabs in riverbeds (Fig. 2c) in Banefo. They display gray color and a granular texture with a slightly porphyritic tendency, punctuated by a few larger K–feldspar crystals. Biotite and muscovite are finely distributed within the lighter phases. The abundance of light–colored minerals gives the rock a leucocratic character. In thin sections (Fig. 2d, the mineral assemblage is dominated by quartz (40%), potassium feldspar (20%), and plagioclase (15%), associated with biotite (10%) and muscovite (7%), along with opaque minerals.

Biotite Granites

Biotite granites cropout as veins which cut across the two–mica granites or as a slab in riverbeds in Banefo (Fig. 2d). At the outcrop scale, they display light gray to whitish color. In thin section (Fig 2e), it shows a granular texture composed of quartz (35%), plagioclase (30%), potassium feldspar (15%), biotite (10%), and chlorite (5%).

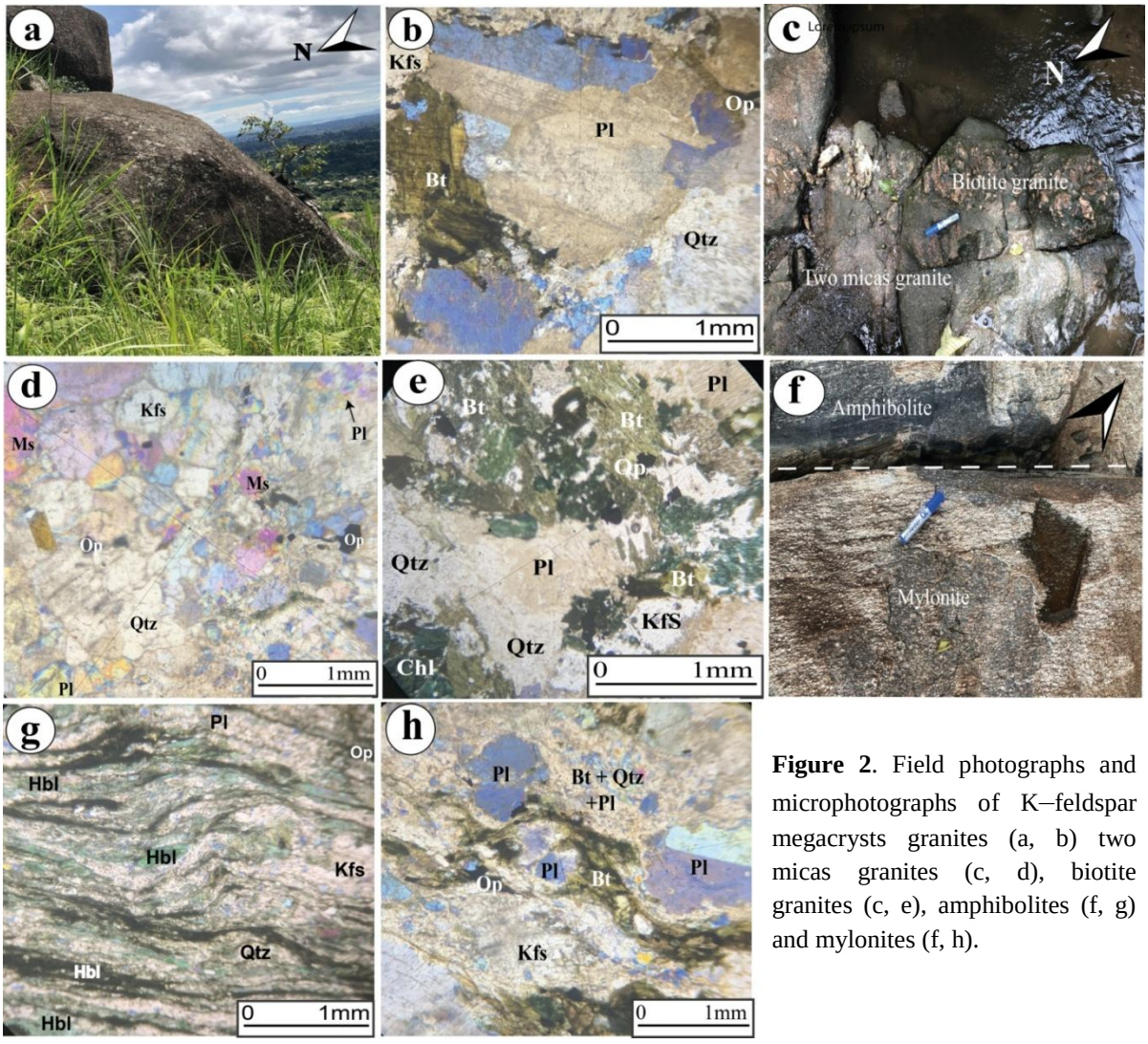

Figure 2. Field photographs and microphotographs of K–feldspar megacrysts granites (a, b) two micas granites (c, d), biotite granites (c, e), amphibolites (f, g) and mylonites (f, h).

Amphibolites

Amphibolites cropout mainly as dark colored enclaves but also as veins within mylonites in Baleng and Gouache (Fig. 2f). It exhibits marked bedding, linked to the alternation of layers respectively rich in amphibole and quartz and K–feldspar. In thin section, the amphibolites display a foliated to nematoblastic texture, characterized by alternating dark and light layers (Fig. 2g). The mineralogical assemblage is dominated by amphibole (45%), plagioclase (20%), quartz (15%), potassium K–feldspar (7%), and biotite (5%).

Mylonites

Mylonites cropout as light gray to dark gray slabs in riverbeds or as blocks on hillsides in Gouache. In Baleng, they are mainly observed in a quarry where they form well–exposed corridor (Fig. 2f). The grain size is fine, a consequence of the dynamic recrystallization of the

minerals, but elongated K–feldspar porphyroblasts are visible (Fig. 2f.). Based on the intensity of deformation recorded in the Gouache and Baleng outcrops, two types are distinguished: protomylonites and ss mylonites. Protomylonites in thin sections exhibit a porphyroblastic texture mainly composed of plagioclase (40%) and quartz (25%), associated with a significant fraction of oriented biotite (15%) and K–feldspar porphyroblasts (10%). Ss mylonites in thin section display heterogranular, predominantly exhibiting a porphyroblastic texture. The porphyroblasts, mainly K–feldspar (20%), are embedded in a foliated matrix of polycrystalline aggregates of quartz (40%), plagioclase (10%) associated with biotite sheets (9%) (Fig. 2h).

IV.3. Metallogenic Potential

Geochemical studies show that the rocks in the Bafoussam area are, on the one hand, biotite-K-feldspar megacrysts type I granitoids, and on the other hand, two–mica type–S granitoids. These rocks exhibit a metaluminous to slightly peraluminous character for the I–type sequences, and a slightly to strongly peraluminous character for the S–type sequences, with a calc–alkaline characteristic particularly in the biotite and two–mica granites [14].

The Fe_2O_3/FeO versus FeOt diagram from [24] shows that the analyzed rocks occupy the "oxidized" domain. Only two biotite granites samples and one mylonites sample occupy the strongly oxidized domain (Fig. 3a). The Rb vs K_2O diagram from [25] (Fig. 3b) shows that the samples belong to the domain of unspecialized granites. This suggests that the analyzed rock samples are generally barren.

Sn–W–Cu–Mo Mineralization

The degree of differentiation and the oxidation state of the magma that gave rise to the granitoids are essential parameters for evaluating their metallogenic potential [26]. The Bafoussam granitoids exhibit SiO_2 contents ranging from 62.03% to 73.82% and K_2O contents from 2.57% to 6.41% [14], typical values of highly evolved calc–alkaline granites, comparable to those of Sn–W granites [27, 28] and K/Rb ratios between 0.0008057 and 0.025459 [14], reflecting a high degree of magmatic differentiation. All these characteristics suggest a highly evolved and weakly oxidized magma, consistent with a I–type peraluminous signature. Such granites are generally associated with Sn, W, U, Li, and rare earth element (REE) mineralization [26, 28]. However, the Sm/Eu vs. Rb diagram in Figure 3c shows that the analyzed granitoids are poor in Sn. [29] used the Rb/Sr vs. Rb/Sr. Color Index diagram uses to differentiate the granitoids and identify their economic potential for Sn–Mo–Cu shows that samples are productive in Cu and Mo, specifically the two–mica granites and mylonites (Fig. 3d).

Zn and Sn mineralization

[30] and [31] highlighted a relationship between SiO_2 content and Zn concentration in granites: the Zn content remains stable (85 ppm) in intermediate rocks, then decreases linearly beyond 60% to reach approximately 35 ppm at 75% SiO_2 [14].

The analyzed rocks contain Zn with concentrations ranging from 21 to 80 ppm [14]. Furthermore, according to [30], rocks containing more than 10% Fe are good targets for Zn prospecting. In the Fe_2O_3t vs. SiO_2 discrimination diagram, samples predominantly occupy the barren field (Fig. 3e), except for one sample of K–feldspar megacryst granites which occupies the fertile zone. In the Zn vs. SiO_2 diagram, samples predominantly plot in fertile field with respect to zinc (Fig. 3f).

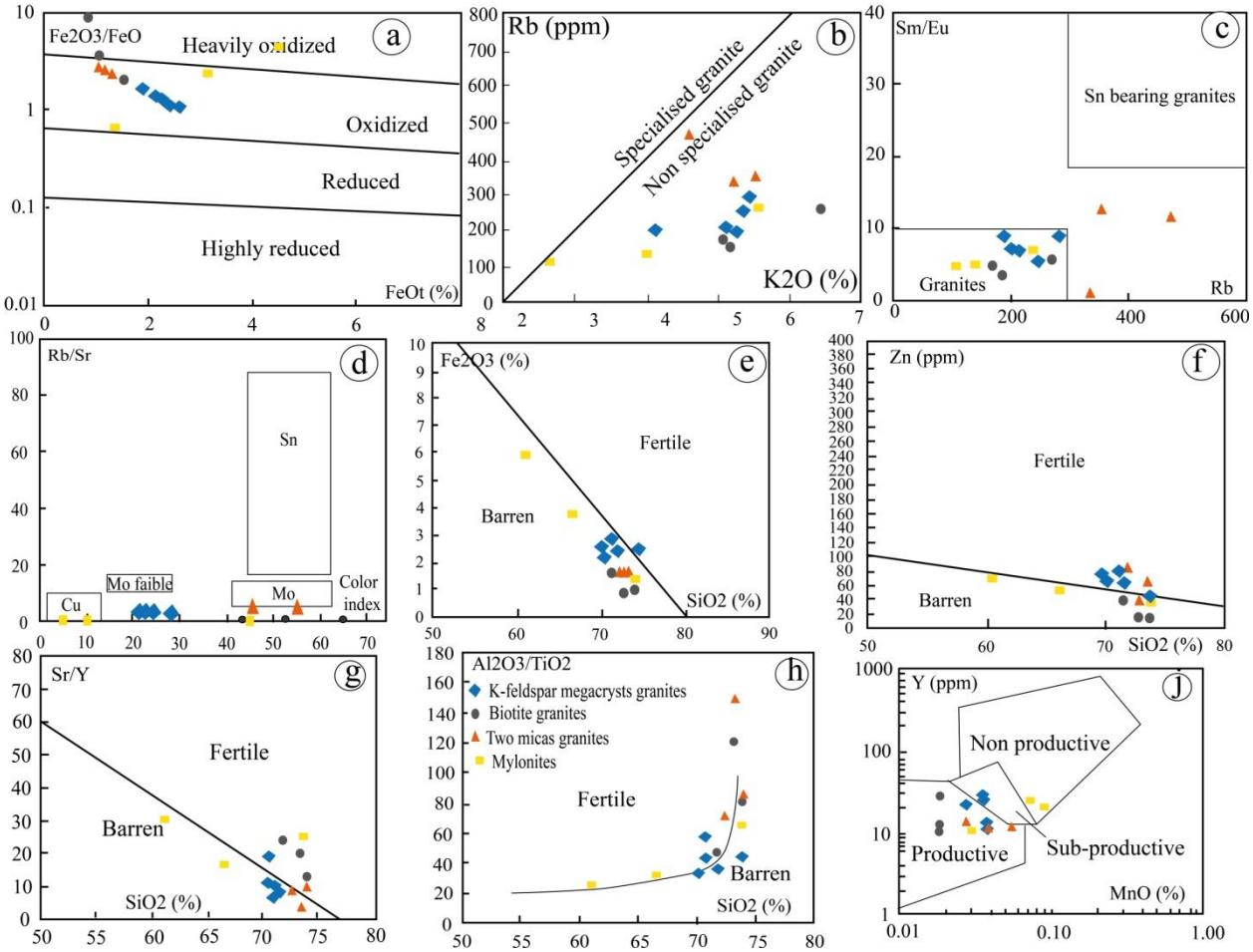

Figure 3. Discrimination diagrams for fertile and barren granites within the Bafoussam granitoids. (a) Fe_2O_3/FeO vs FeOt after [24]; (b) Rb vs. K_2O [25]; (c) Sm/Eu vs. Rb; (d); Rb/Sr vs. CI after [29]; (e) Fe_2O_3 vs. SiO_2 after [30], (f) Zn vs. SiO_2 after [30]; (g) Sr/Y vs. SiO_2 after [32]; (h) Al_2O_3/TiO_2 VS. SiO_2 after [32]; (j) Y vs. MnO after [33].

Cu Mineralization

The evaluation of the copper mineralization potential, using the Sr/Y and Al_2O_3/TiO_2 versus SiO_2 diagrams of [28], shows that K–feldspar megacryst granites, two–mica granites, biotite granites, and mylonites overlap the fertile and sterile field (Fig. 3gh), suggesting copper mineralization [32]. In the Y = f(MnO) diagram of [33], samples plot in all three fields (Fig. 3j): productive, unproductive, and sub–productive. It is worth noting that only two–mica granites and biotite granites are predominantly productive.

Skarn Mineralization

Skarn–type mineralizations are generally associated with calc–alkaline or metalluminous granitic intrusions characterized by low aluminum contents [34]. In the study area, the analyzed samples exhibit SiO_2 concentrations generally higher than those reported in typical granites associated with Fe–Cu–Au skarn deposits [34]. When these data are plotted on the Na_2O+K_2O vs. SiO_2 diagram, samples are close to fields of rocks associated with Mo–Sn–Zn skarn systems (Fig. 4a). Furthermore, the Nb vs. Y of Figure 4b and Rb vs. (Y + Nb) of Figure 4c reveal that the granites compositions are close to those of Cu–, Mo–, Sn–rich and skarn–rich granitoids. However, not all samples within the skarn–associated granitoid range exhibit systematic enrichments in base

metals such as Cu–Pb–Th–Zn. The most common skarn–related minerals in the study area are Cu and Mo.

Th–U and rare metal mineralization

Th–U Mineralization

Th–U mineralization develops in the upper continental crust, particularly in placer deposits and veins. In the study area, samples exhibit high U (8–11 ppm) and Th (8–70 ppm) contents [14] compared to the upper continental crust (U = 2.7 ppm, Th = 10.5 ppm [35]. These enrichments reflect the fractionation of U and Th in accessory minerals such as zircon, monazite, allanite, and apatite [14, 36]. The Th vs. U diagram of Figure 4d suggests fractionation and possible leaching during magmatic differentiation. Th/U ratios (2.375–7) generally exceed that of the continental crust (~4), indicating that U is mostly trapped in refractory accessory minerals. Only samples with Th/U < 1 show a proportion of mobilizable U [37, 38]. Thus, despite their U contents being higher than the crustal average, the granites in the study area are not good hosts for uranium mineralization, as U is fractionated by in poorly soluble phases. The evaluation of the metallogenic potential based on the P_2O_5*100/Th ratio vs. B (B = Ti + Fe + Mg) (Fig. 4e) according to [39], shows that the Th–mineralized rocks are rich in P/Th and exhibit an evolutionary trend parallel to the Y–axis. The Bafoussam granites display a sub–vertical trend and are sub–parallel to the Y–axis, suggesting that they are potentially Th–mineralized.

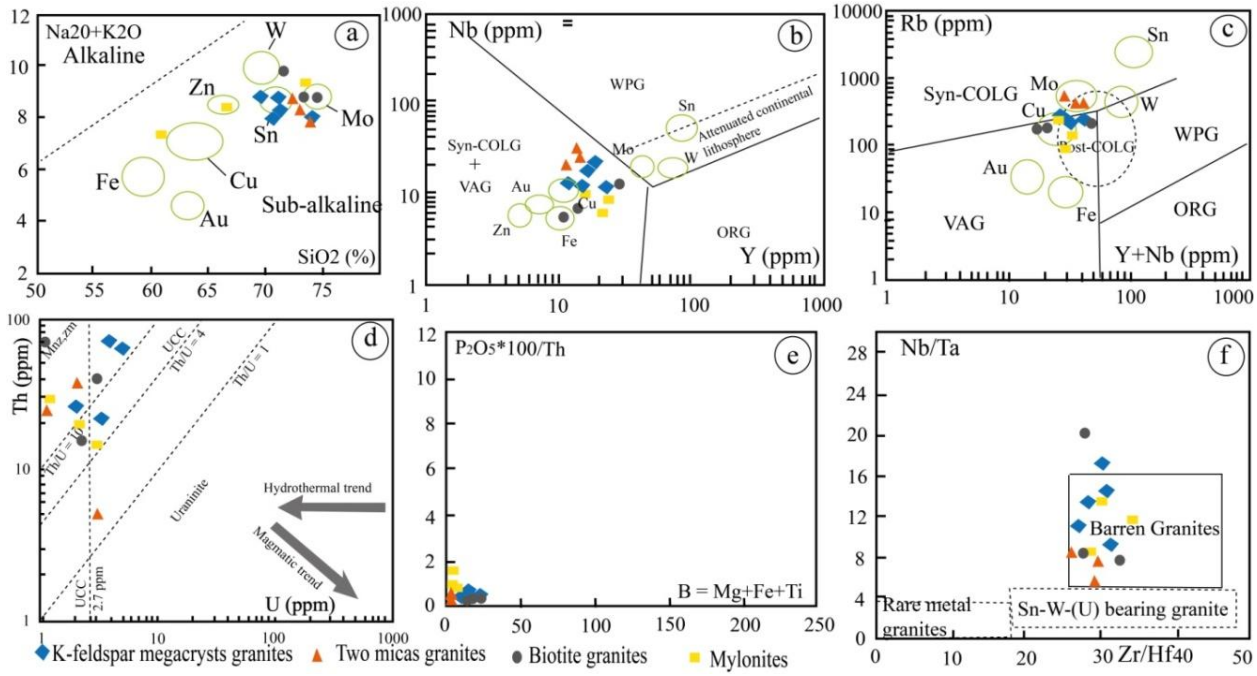

Figure 4 Binary plots and potentiality in Cu, W, Zn, Sn, Mo and Th–U in the Bafousam granitoids. (a) K_2O+Na_2O vs. SiO_2 after [34]; (b) Nb vs. Y after [34]; (c) Rb vs. (Y + Nb) after [34]; (d) Sr/Y vs. SiO_2 (wt.%) after [32]; (e) Y vs. MnO (wt.%) after [33]; (f) Th vs. U; (e) P_2O_5 x 100/Th vs. Mg + Fe + Ti ; (f) Nb/Ta vs.Zr/Hf after [39].

Rare Earth Element (REE) Mineralization

The studied rocks show a progressive increase in total rare earth element contents (∑REE) as well as a significant increase in normalized (La/Lu)N ratios (Fig. 5a). This geochemical signature is characteristic of a normal magmatic differentiation process. A clear negative relative correlation between SiO_2 and ∑HREE contents is observed (Fig. 5b), indicating that magmatic evolution towards more acidic granites is accompanied by a depletion of heavy rare earth

elements. This phenomenon reflects fractionation in selective magmatism, where early mineral phases crystallize and are removed from the magma, altering the residual composition of the magmatic fluid. Similarly, the ∑REE and ∑HREE vs. SiO_2 diagrams (Figs. 5c–d) also show a negative trend, reflecting a progressive evolution of the magma through the partial removal of LREE–rich minerals such as monazite or allanite. Based on the above observations, rocks in the study area resulted from normal magmatic differentiation devoid of magmatic fluid, leading to HREE depletion.

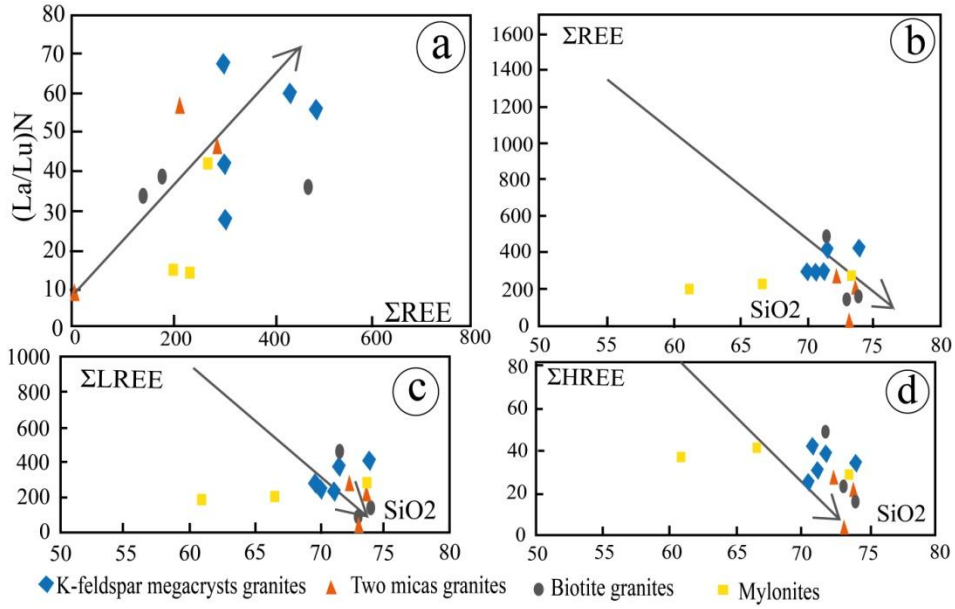

Figure 5. Discrimination diagrams of REE in the Bafoussam granitods. (a) La/Lu vs. ∑REE ; (b) ∑REE vs. SiO_2 ; (c) ∑LREE vs. SiO_2 ; (d) ∑HREE vs. SiO_2.

IV.3. Statistical analysis for metallogenic potential

The objective of this analysis is to identify anomalies based on threshold values defining the lower and upper limits of a dataset. These thresholds serve to differentiate normal variations observed within a given population from outliers. Thus, values between these limits are considered representative of the geochemical background, while those that deviate from them, either upwards or downwards, indicate significant anomalies. In mineral exploration, attention is generally focused on positive anomalies, interpreted as reflecting enrichment in elements linked to the presence of mineralization or to secondary leaching processes that have concentrated certain metals beyond their average crustal content. However, negative anomalies also deserve consideration, as they can signal localized depletion of certain elements resulting from alteration processes in the host rocks, often associated with the emplacement of mineralization [40]. Histogram representations reveal a marked asymmetry in the distribution of mineralization indices in the studied rocks (Fig. 6), with dominant multimodal distribution. The analysis of these representations allows for several observations: (i) the bars located towards the left of the histogram corresponding to samples whose concentrations are less than reference threshold; (i) median bars corresponding to samples whose concentrations are around the normal crust values and (iii) the bars located towards the right of the histogram corresponding to samples whose concentrations approach or exceed the reference threshold, thus identifying geochemical anomalies (Figs. 6a–c).

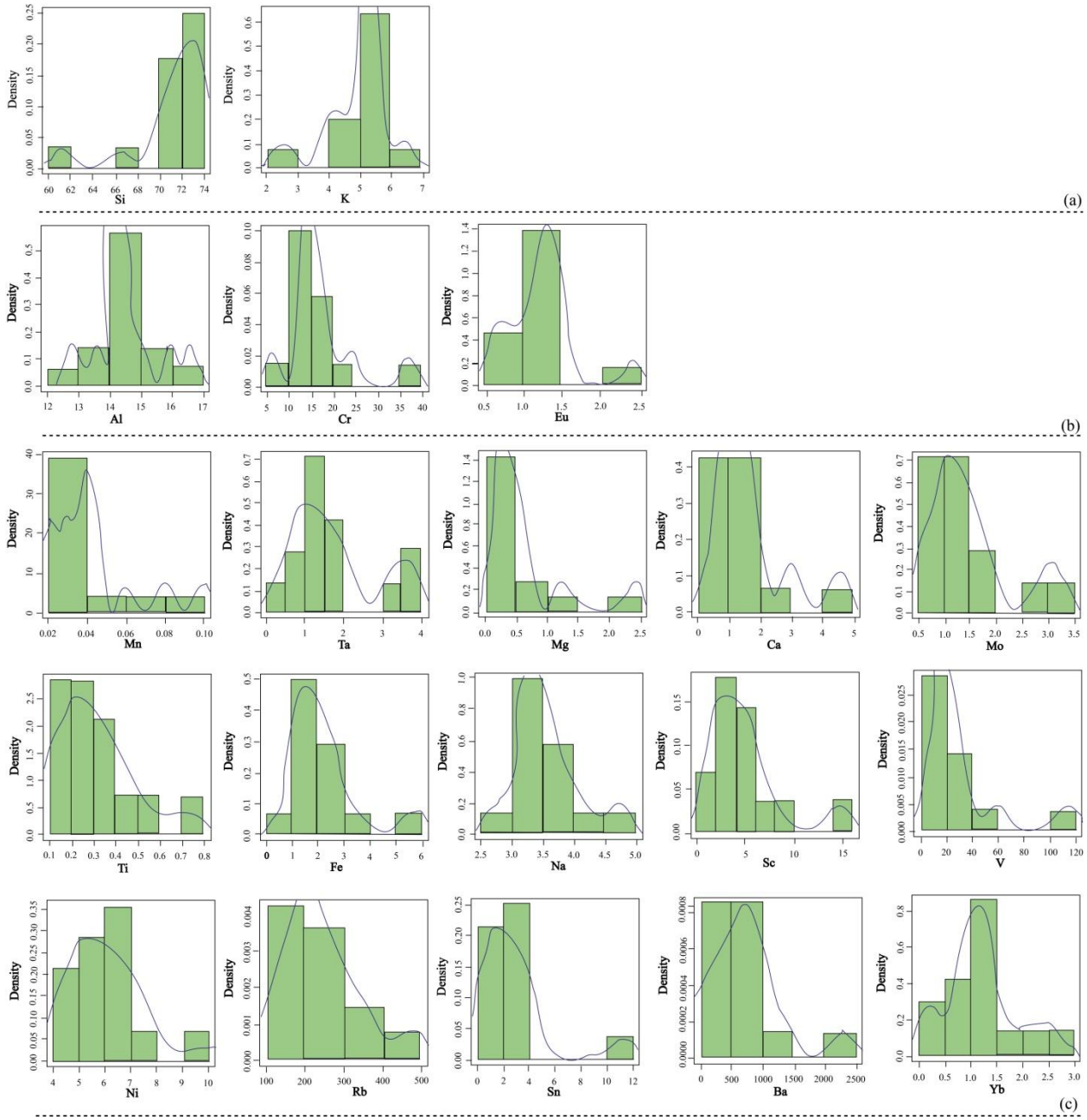

Figure 6. Histograms showing the distribution of elements within rocks of the study area.

Box plot representations show that the small circles are concentrated towards the left for Si, K (Fig. 7a), suggesting that their concentrations are below the critical threshold [12]. For Al, Cr and Eu, the distribution shows multiple populations illustrated by circles concentrated to the left and right (Fig. 7b), reflecting the geochemical heterogeneity of the samples and typical of natural geochemical data [41, 42]. For Mn, Ta, Mg, Ca, Mo, Ti, Fe, Na, Sc, V, Ni, Rb, Sn, Ba and Yb, circles are represented to the right suggesting that their concentrations are above the critical threshold.

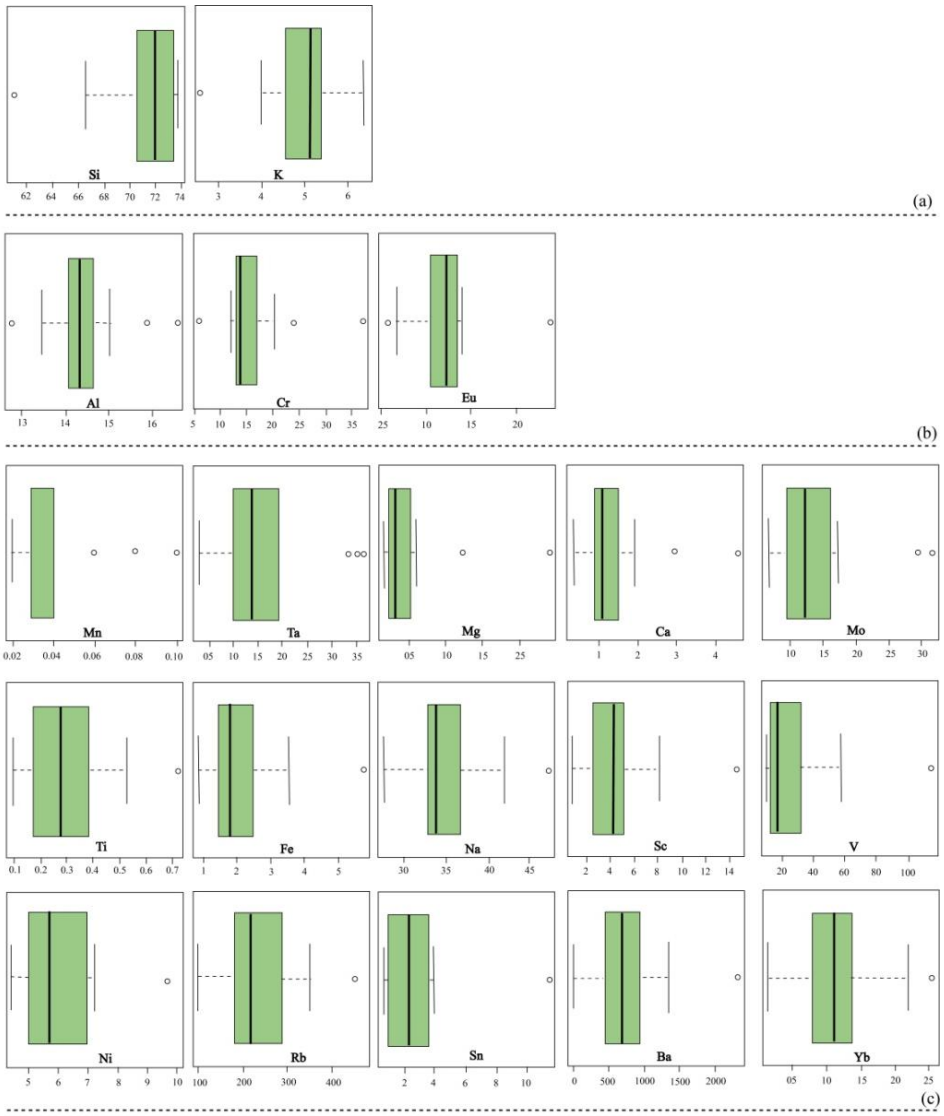

Figure 7. Box-plots showing major, REE and trace metal concentration variation and anomalies within rocks of the study area.

According to the calculated thresholds (Table 1), certain elements (e.g., Rb, Mo, Ta, Sn, Ba, Eu, and Yb) show positive anomalies relative to the maximum measured concentrations (Fig. 7). The analyzed rocks exhibit enrichment in Si, K, Al, Cr, Eu, Mn, Ta, Mg, Ca, Mo, Ti, Fe, Na, Sc, V, Ni, Rb, Sn, Ba, and Yb, reflecting geochemical anomalies (Fig. 7).

V. Discussion

V.1. Petrography: Emplacement chronology

Petrographic data show that the study area is composed of K–feldspar megacrysts granites, two-mica granites, biotite granites, amphibolites, and mylonites. The K–feldspar megacryst granites are the oldest; the two–mica granites outcrops as a slab and is cut across by biotite granites veins (Fig. 2c); amphibolites appear as lense–like enclaves within mylonites (Fig. 2a), indicating later emplacement of mylonites. Mylonites result from solid–state recrystallization of granites under the control of an active shear zone, the CCSZ, during the Pan–African orogeny [8, 9]. These mylonites exhibit a low proportion of clasts in favor of a high concentration of blasts (Figs. 2h).

These data show that granites were essentially mylonitized while still warm [44]. The emplacement chronology of these rocks, from oldest to youngest, is as follows: amphibolites – K–feldspar megacryst granites – two mica granites – biotite granites – mylonites.

Table 1: Statistical data of major and trace elements concentration in both granites from the study area. The Clarke values are after [43]. Elts =Elements; n =Number of samples; Av =Average; Min =Minimum; Max =Maximum; Q =Quartile; Thr =Threshold.

Elements/metals	n	Av	Min	Q_1	Q_2	Q_3	Max	Thr	Clarke
Si	14	71.2	61.03	70.83	72.02	73.47	73.82	77.43	28.8 (Wt%)
Ti	14	0.31	0.1	0.19	0.28	0.38	0.72	0.665	0.401 (Wt%)
Al	14	14.47	12.81	14.12	14.34	14.61	16.6	15.345	7.96 (Wt%)
Fe	14	2.18	0.88	1.45	1.81	2.44	5.79	3.925	4.32 Wt%)
Mn	14	0.04	0.02	0.03	0.04	0.04	0.1	0.055	0,07 (Wt%)
Mg	14	0.55	0.19	0.23	0.3	0.52	2.41	0.955	2.2 (Wt%)
Ca	14	1.49	0.37	0.9	1.11	1.53	4.59	2.475	3.85 (Wt%)
Na	14	3.53	2.78	3.28	3.38	3.66	4.71	4.23	2.36 (Wt%)
K	14	4.94	2.57	4.69	5.16	5.4	6.41	6.465	2.14 (Wt%)
Ba	14	735.24	6.81	459.5	688.5	953.75	2324	1695.125	584 (ppm)
Sc	14	4.63	0.82	2.48	4.2	5.18	14.6	9.23	16 (ppm)
V	14	29	11	13	18	30	115	55.5	98 (ppm)
Cr	14	16.29	6.07	13	14	16.75	37	22.375	126 (ppm)
Ni	14	6.11	4.48	5.04	5.72	7	10	9.94	90 (ppm)
Rb	14	241	101	183	218	280	470	425.5	78 (ppm)
Mo	14	1.42	0.68	0.97	1.23	1.57	3.16	2.47	1.1 (ppm)
Ta	14	1.71	0.32	1.02	1.4	1.91	3.66	3.245	1.1 (ppm)
Sn	14	2.78	0.68	0.99	2.25	3.49	11.4	7.24	2.3 (ppm)
Eu	14	1.32	0.57	1.06	1.25	1.38	2.4	1.86	2.1 (ppm)
Yb	14	1.18	0.16	0.83	1.14	1.34	2.55	2.105	2 (ppm)

IV.3. Metallogenic Implications

Research works from of [14] shows that the Bafoussam granitoids have a calc–alkaline, metaluminous character, typical of I– and S–type granitoids. These rocks are potentially fertile for Sn, W, Cu, Mo, Zn, Th, and rare earth mineralization, but sterile for certain epithermal metals (Figs. 4). The comparison of the elemental and metal content of metallogenic interest in the studied rocks with their natural abundance in the continental crust (Clarke) (Table 1) shows significant enrichments in Si, Ti, Al, Fe, Mn, Mg, Ca, Na, K, Sc, V, Cr, Ni, Rb, Mo, Ta, Sn, Ba, Eu, and Yb. These enrichments result from magmatic differentiation and hydrothermal rock–fluid interactions linked to mylonitization and the emplacement of plutonic massifs, sources of heat and magmatic fluids [45].

The positive and negative geochemical anomalies observed on the histograms and box plots (Figs. 6 and 7) confirm these processes. Mn, Ta, Mg, Ca, Mo, Ti, Fe, Na, Sc, V, Ni, Rb, Sn, Ba, and Yb positive anomalies (Figs. 6c and 7c) indicate a mixed source of mineralization,

originating from both the protolith and accumulations in its environment [41]. Mafic elements (Fe, Mg, Ti, Mn, Ni, V, Sc) are mainly carried by ferromagnesian and accessory minerals such as biotite (Figs. 2d–e) and amphibole (Fig. 2g), while the alkaline elements (Na, Ca, Rb and Ba) are mainly concentrated in plagioclase (Figs. 2b, d–e, g–h), K–feldspar (Figs. 2d–e)) and the micas (Figs. 2d–e, h). Finally, the incompatible elements (Ta, Sn, Mo and Yb) are mainly found in late accessory minerals such as zircon and monazite. The negative and positive anomalies in Al present in aluminous phases such as micas and K–feldspar (Figs. 2d–e), in Cr present in mafic minerals such as amphiboles (Fig. 2g) and in Eu which crystallizes in plagioclase (Figs. 2b, d–e, g–h), are linked to metamorphic effects following the increase in temperature and pressure [45]. This thermal and barometric rise would promote the leaching of certain metals during the dehydration of minerals [2, 46]. On the other hand, the strictly negative anomalies observed in Si and K (Figs. 6a and 7a) would be linked to lithogenesis [45, 47], with Si crystallizing in quartz (Figs. d–e) and K in K–feldspar (Figs. 2d–e). These mineralogical associations are consistent with the advanced magmatic differentiation of the granitoids in the studied area. Faults and fractures act as hydrothermal conduits, controlling the emplacement and spatial distribution of the mineralizations. All of these indicators show that in the Bafoussam area, rocks display significant metallogenic potential. The Central and Western domains of the CAFB therefore warrant exploration due to their high potential for base metals and rare earth elements.

Conclusion

Field and laboratory studies show that the area under examination is composed of various rock types, including K–feldspar megacryst granites, two–mica granites, biotite granites, amphibolites, protomylonites, and mylonites. Metallogenic analyses indicate that the samples predominantly plot in the oxidized field encompassing both unspecialized zones, suggesting that they are barren. Some granites and mylonites samples particularly show significant potential for skarn formation. Furthermore, these rocks exhibit moderate rare earth element (REE) content, with a depletion of heavy REEs (HREE), limiting their potential for light REEs (LREE). Statistical analysis, corroborated by histogram examination, reveals an asymmetrical distribution, characterized by a high concentration of low values and the marginal presence of samples displaying higher values. Statistic data highlights mineralization potential for Mn, Ta, Mg, Ca, Mo, Ti, Fe, Na, Sc, V, Ni, Rb, Sn, Ba, and Yb, thus underscoring the geological and metallogenic importance of the studied area.

References

[1] Fozing, E. M., Tcheumenak Kouémo, J., Sawadogo, S., Tchamabe, B. C., Safianou, O., Koagne, Foka, S., Nguimezap, M. M., Kwekam, M. (2024). Intergrating geospacial data and multi–criteria analysis for mapping and evaluating the mineralization potential of the Dschang pluton (Western Cameroun). Earth Sciences Informatics. https://doi.org/10.1007/s12145-024-01475-4.

[2] Fozing E.M., Chako Tchamabé B., Tcheumenak Kouémo J. Njomouo Njiojob F. J., Kamnang Fotso D., Achu Megnemo L., Kwékam M., Njonfang E. (2026). Evidence of polyphase deformation and metallogenic anomalies significance in the Batié Pluton (West Cameroon): Constraints from field observations and geochemical statistical analysis. Journal of African Earth Sciences 238, 106084.

[3] Fozing, E. M., Kwekam, M., Tcheumenak Kouemo, J., Njanko, T., Njonfang, E. (2021). Kinematic analysis of the Dschang granitic pluton (West–Cameroun): Implications of the pan–African deformation of the central of the Central African fold belt in Cameroun during the post–

collisional history of western Gondwana. Precambrian Research, 359, 106231. https://doi.org/10.1016/j.precamres.2021.106231.
[4] Kwékam, M., Liégeois, J. P., Njonfang, E., Affaton, P., Hartmann, G., Tchoua, F. (2010). Nature, origin and significance of the Fomopea Pan-African high–K calc-alkaline plutonic complex in the Central African fold belt (Cameroon). Journal of African Earth Sciences, 57, 79–95.
[5] Kwékam, M., Hartmann, G., Njanko, T., Tcheumenak, Kouémo, J., Fozing, E. M., Njonfang, E. (2015). Geochemical and isotope Sr–Nd character of Dschang biotite granite: Implications for the Pan–African continental crust evolution in WestvCameroon (Central Africa). Earth science Research, 4(1), 88–102.
[6] Kwékam M., Dunkl I., Fozing E. M., Hartmann G., Njanko T., Tcheumenak K. J., Njonfang E. (2020a). Syn-kinematic ferroan high–K I–type granites from Dschang in southwestern Cameroon: U–Pb age, geochemistry and implications for crustal growth in the late Pan–African orogeny. Geological Society, London, Special Publications, 502.
[7] Kwékam, M., Talla, V., Fozing, E. M., Tcheumenak Kouémo, J., Dunkl, I., Njonfang, E. (2020b). The Pan–African High–K I–Type Granites from Batié Complex (West-Cameroon): Age, Origin and Tectonic Implications. Frontiers in Earth Sciences 8 (363).
[8] Tcheumenak K. J., Njanko, T., Kwékam, M., Naba, S., Bella, Nke, B. E., Yakeu, Sandjo, A. F., Fozing, E. M., Njonfang, E. (2014). Kinematic evolution of the Fodjomekwet-Fotouni shear zone: Implication for emplacement of the Fomopéa and Bandja plutons. Journal of Africa Earth Sciences, 99: 261–275.
[9] Tcheumenak Kouemo, J., E. M. Fozing, H. Zagalo Al–Hadj, Noudiedie Kamgang, J. A. Kwekam, M. and Njonfang., E. (2023). "Structural and Petrographic Characterization of the Fotouni–Kekem Shear Zone: Implication for P–T–t Regional Metamorphism and Mylonitic Evolutions Along the Central Cameroon Shear Zone." Arabian Journal of Geosciences 14: 1497. https://doi.org/10.1007/ s12517-022-11095-1.
[10] Tcheumenak, Kouémo, J., Sobze, Yemdji, B. R., Fozing, E. M., Tepi, Yemele, B. R., Azefack, Mbounou, R. L., Kwékam, M. (2024). Petrogaphic and structural analyses of high-grade amphibolites from Fotouni–Kékem and Nyakong–Manyi shear zones: implications for the geodynamic signifcance of the Central Cameroon Shear Zone. Environnemental Earth Sciences, 523: 2–23.
[11] Yannah, M., Fodoue, Y., Kwékam, M., Mbassa, B.J., Tifang Amboh, J., Kagou Dongmo, A., Ayonghe Ndonwi, S., 2022. Geochemical evaluation of mineralization potential of the SomieNtem area within the tikar plain, Cameroon: implication on petrogenesis. Acta Geoch 41, 861–886.
[12] Toteu, S. F., Van Schmus, W. R., Penaye, J., Michard, A. (2001). New U– Pb and Sm–Nd data from north–central Cameroon and the pre–Pan African history of central Africa. Precambrian Research 108, 45–73.
[13] Ngako, V., Affaton, P., Njonfang, E. (2008). Pan–African tectonic in north-western Cameroon: implication for history of western gondwana. Gondwana Res. 14, 509–522.
[14] Djouka–Fonkwé, M. L., Schulz, B., Schussler, U., Tchouankoue, J. P., Nzolang, C. (2008). Geochemistry of the Bafoussam Pan–African I– and S–type granitoids in western Cameroon. Journal of African Earth Sciences, 50 (2–4), 148–167.
[15] Njiékak, G., Dorr, W., Tchouankoué, J. P., Zulauf, G. (2008). U–Pb zircon and micro-fabric data of (meta) granitoids of western Cameroon: Constraints on the timing of pluton emplacement and deformation in the Pan–African belt of central Africa. Lithos, 102(3–4), 460–477.

[16] Njiékak, G., Ngako, V., Tchouankoue, J. P., Dorr, W. (2015). Chronology of tectonic events in the Pan–African belt of western Cameroon: Constraints from structural geology and U–Pb zircon geochronology of syn–to post–kinematic granitoids. Journal of African Earth Sciences, 108, 1–16.
[17] Njiékak, G., Efon–Ekang, E. R., Ngako, V., Yonta–Ngoune, C., & Ndong Bidzang, B. (2020a). Geochemistry and U–Pb Zircon Geochronology of the Batie Granitoids (West Cameroun): Constraints on the Crustal Evolution in the Pan-African Belt. Geosciences, 10(10), 406.
[18] Safianou, O., Fozing, E. M., Tcheumenak Kouemo, J., Achu Megnemo, L., Kamgang Tchuifong, A. B., Aman, S., Mohamed, R., Kwékam, M. (2024). Mapping and discrimination of the mineralization potential in granitoids from the Banyo area (Adamawa, Cameroon) using Landsat 9 OLI, ASTER images, and field observations. Geosystems and Geoenvironnement, 3: 100239.
[19] Pemha Nyemb Sayoum, L. C., Ngos, S., Basse, E. N., Ganno, S., Owona, S., & Njopwopam, K. (2024). Mineralogical and geocgemical features or rare earth elements (REE) in the Bafoussam granitoids (West Cameroon): Implication for REE mineralization potential. Journal of African Earth Sciences, 216, 105273.
[20] Nguema, R. F., Ngono, M. C., Ongoundou, P. S. (2023). Mineral potential of iron and manganese deposits in Central Africa: A review. Journal of African Earth Sciences, 201, 104880.
[21] Ghodsi, M. T., Sadeghi, B., & Esfahani, A. F. (2016). Geochemical discrimination of fertile and barren granites in the Urumieh–Dokhtar Magmatic Arc, Iran. Journal of African Earth Sciences, 124, 1–15.
[22] Janoušek, V., Farrow, C. M., Erban, V. (2006). Technical Note – Interpretation of Whole–rock Geochemical Data in Igneous Geochemistry: Introducing Geochemical Data Toolkit (GCDkit). Journal of Petrology 47 (6), 1255-1259.
[23] Yusta, I., Velasco, F., Herrero, J.M. (1998). Anormaly threshold estimation and data normalisation using EDA statistics: application to lithogeochemical exploration in lower 254 Cretaceous Zn–Pb carbonate-hosted deposits, Northern Spain. Applied Geochemistry 13 (4), 421–439.
[24] Champion, D. C., Heinemann, K. (1994). Fe_2O_3/FeO ratio and its relationship to the oxidation state of granitic magmas. Journal of petrology, 35(5), 125–138.
[25] Tuach, J., Henderson, P., Rogers, G. (1986). The Rb–K_2O systematic of granitic rocks: a tool for recognizing specialized granites. Mineralium Deposita, 21(3), 191–199.
[26] Blevin, P. (2003). Metallogeny of granitic rocks. In: Magmas to mineralization. Blevin P et al. (eds). The Ishihara symposium, pp 1–4.
[27] Ramirez, J.A. Grundvig, S. (2000). Causes of geochemical diversity in peraluminous granitic plutons: The Jálama Pluton, Central–Iberian Zone (Spain and Portugal). Lithos 50, 171–190.
[28] Rossi, J.N., Toselli, A.J., Saavedra, J., Sial, A.N., Pellitero, E. Ferreira, V.P. (2002). Common crustal sources for contrasting peraluminous facies in the early Paleozoic Capillitas Batholith, NW Argentina. Gondwana Research 5, 325–337.
[29] Karimpour, M. H., Bowes, W. W. (1983). Application of trace elements and isotopes for discriminating between porphyry molybdenum, copper, and tin systems and the implications for predicting the grade. Global Tectonic Metallogeny 2, 1–16.

[30] Wolfe, W.J. (1977). Geochemical exploration of early Precambrian volcanogenic sulphide mineralization in Ben Nevis Township, District of Cochrane: Ontario. Geological Survey Study 19 (39).
[31] Lentz, D. R. (1998). Petrogenetic and geodynamic implications of extensional regimes in the phanerozoic subduction zones and their relationship to VMS–forming systems. Ore Geology Review 12, 289–327.
[32] Loucks, R. R. (2014). Distinctive composition of copper–ore forming arc magmas. Australian Journal of Earth Sciences 61, 5-16.
[33] Baldwin, J. A. and Pearce, J. A. (1982). Discrimination of igneous rock types and tectonic settings by their MnO–Y relationships. Chemical Geology, 37, 335–343.
[34] Meinert, L. D., Dipple, G. M., Nicolescu, S. (2005). World skarn deposits. In: Hedenquist, J.W., Thompson, J.F.H., Goldfarb, R.J., Richards, J.P. (Eds), Economic Geology, 100th Anniversary Volume. Society of Economic Geologists, Littleton, CO, pp. 299–336.
[35] Rudnick, R. L., Gao, S. (2003). Composition of the continental crust. Treatise in Geochemistry 3, 1–64.
[36] Bea, F. (1996). Residence of REE, Y, Th and U in granites and crustal protoliths: implications for the chemistry of crustal melts. Journal of Petrology 37, 521–552.
[37] Friedrich, M., Cuney, M., Poty, B. (1987). Uranium geochemistry in peraluminous leucogranites. Uranium 3, 353–385.
[38] Cuney, M. (2014). Felsic magmatism and uranium deposits. Bulletin de la Société Geologique Française 185, 75–92.
[39] Scheepers, R. (2000). Granites of the Saldania mobile belt, South Africa: radioelements and P as discriminators applied to metallogeny. Journal of Geochemical Exploration 68, 69–86.
[40] McQueen, K.G. (2008). Identifying geochemical anomalies. CRC LEME, pp. 1–7.
[41] Reimann, C., Filzmoser, P. (2000). Normal and lognormal data distribution in geochemistry: death of a myth. Consequences for the statistical treatment of geochemical and environmental data. Environmental Geology 39, 1001–1014.
[42] Reimann, C., Filzmoser, P., Garrett, G. (2005). Background and threshold: critical comparison of methods of determination. Science of the Total Environment 346, 1–16.
[43] Wedepohl, K.H. (1995). The composition of the continental crust. Geochimica and Cosmochimica Acta 59, 1217–1232.
[44] Efon Awoum, J., Fozing, E.M., Kwékam, M., Tcheumenak Kouémo, J., Choumele Kana, S.C., Achu Megnemo, L. (2020). Structural characterization of the Pan–African Ndiéki area in the Foumban–Bankim Shear Zone (West Cameroon): constraints from field observations and microstructures. Arabian Journal of Geosciences 13: 831.
[45] Zuo, R.G. (2021). Mineral Exploration Using Subtle or Negative Geochemical Anomalies. Journal of Earth Science 32 (2), 439–454.
[46] Möller, P., Bau, M., Dulski, P., Lüders. (12–18 August 1998). V. REE and Yttrium Fractionation in Fluorite and Their Bearing on Fluorite Formation. In Proceedings of the Ninth Quadrennial IAGOD Symposium, Beijing, China, pp. 575–592.
[47] Shi, C. Y., Wang, C.F. (1995). Regional Geochemical Secondary Negative Anomalies and their Significance. Journal of Geochemical Exploration, 55 (1/2/3), 11-23.